Journal of Computational Physics 351 (2017) 455–472

Contents lists available at ScienceDirect

Journal of Computational Physics

www.elsevier.com/locate/jcp

A multidimensional unified gas-kinetic scheme for radiative transfer equations on unstructured mesh

Wenjun Sun [a], Song Jiang [a], Kun Xu [b,*]

[a] Institute of Applied Physics and Computational Mathematics, No. 2, FengHao East Road, HaiDian District, Beijing 100094, China
[b] Department of Mathematics and Department of Mechanical and Aerospace Engineering, Hong Kong University of Science and Technology, Clear Water Bay, Kowloon, Hong Kong

ARTICLE INFO

Article history:
Received 15 July 2017
Received in revised form 19 September 2017
Accepted 21 September 2017
Available online 25 September 2017

Keywords:
Radiative transfer equations
Unstructured mesh
Asymptotic preserving
Implicit unified gas kinetic scheme
Nine-point diffusion scheme

ABSTRACT

In order to extend the unified gas kinetic scheme (UGKS) to solve radiative transfer equations in a complex geometry, a multidimensional asymptotic preserving implicit method on unstructured mesh is constructed in this paper. With an implicit formulation, the CFL condition for the determination of the time step in UGKS can be much relaxed, and a large time step is used in simulations. Differently from previous direction-by-direction UGKS on orthogonal structured mesh, on unstructured mesh the interface flux transport takes into account multi-dimensional effect, where gradients of radiation intensity and material temperature in both normal and tangential directions of a cell interface are included in the flux evaluation. The multiple scale nature makes the UGKS be able to capture the solutions in both optically thin and thick regions seamlessly. In the optically thick region the condition of cell size being less than photon's mean free path is fully removed, and the UGKS recovers a solver for diffusion equation in such a limit on unstructured mesh. For a distorted quadrilateral mesh, the UGKS goes to a nine-point scheme for the diffusion equation, and it naturally reduces to the standard five-point scheme for a orthogonal quadrilateral mesh. Numerical computations covering a wide range of transport regimes on unstructured and distorted quadrilateral meshes will be presented to validate the current approach.

1. Introduction

This paper is about the development of a multi-dimensional implicit unified gas kinetic scheme (UGKS) for numerical solution of time-dependent radiative transfer equations on unstructured mesh. For the study of radiation transport through a complicated configuration of different opacity material, the construction of a reliable and accurate method with unstructured mesh is a preferable choice. For a structured mesh, the direction-splitting UGKS has been developed [1,16,18]. It is challenging to extend the method to unstructured mesh with the ability to provide accurate solutions in all regimes including free-streaming and diffusive limits.

The radiative transfer equation is used in astrophysics, inertial confinement fusion, high temperature flow systems. The equations of radiative transfer model, at the kinetic scale, the time evolution of radiative intensity and its interaction with material. The opacity of the background material influences greatly on the behavior of radiation transfer. For a low opacity

* Corresponding author.
E-mail addresses: sun_wenjun@iapcm.ac.cn (W. Sun), jiang@iapcm.ac.cn (S. Jiang), makxu@ust.hk (K. Xu).

https://doi.org/10.1016/j.jcp.2017.09.036
0021-9991/

material, the interaction is weak and the radiation takes free-streaming. On the other hand, due to intensive absorption and emission of photons through a high opacity material, the photon will have a diminishing mean free path and a diffusive transport behavior will emerge. So, the radiative transfer is a multi-scale phenomenon and a corresponding multiple scale method is needed for its accurate simulation.

A direct solver for radiative transfer equation usually requires the mesh size in the physical space be comparable to the photon's mean-free path. In the diffusive regime, a small mean free path enforces a huge computational cost to capture the solution. In order to release the difficulties, to develop asymptotic preserving (AP) scheme for the kinetic equation gets much attention in the algorithm development [5,6,9,10]. For unsteady problems, one type of the AP schemes was constructed based on a decomposition of the distribution function between an equilibrium part and its non-equilibrium derivation [7,8]. A rather different approach, based on the unified gas kinetic scheme (UGKS) framework [2,15], has recently been developed for a linear radiation transport model [13], and for coupled multi-frequency radiation transport equation and material energy equation [1,16,18,20]. All the above approaches are based on the structured quadrilateral mesh. It should be pointed out that the multidimensional methods, based on implicit residual distribution schemes, were also developed for the equations of radiative transfer in [19] on the structured mesh.

The goal of this paper is to further develop the UGKS scheme for radiation transfer equations on unstructured mesh. The scheme has the following features. Firstly, an implicit interface flux is constructed for radiation intensity. As a result, the time step of the scheme is not limited by the CFL condition, and a large time step can be used in simulation. Secondly, in order to develop an accurate solver on unstructured mesh, a multi-dimensional formulation for the flux transport is constructed at a cell interface, where the flow variations in both normal and tangential directions are included in the flux evaluation. With the multidimensional property, the current scheme for unstructured mesh will go to a nine-point scheme (see [17]) for the distorted quadrilateral mesh under diffusive limiting condition, and reduce to a standard five-point scheme for the orthogonal quadrilateral mesh. Thirdly, it can be proved that the UGKS is an asymptotic preserving method which presents accurate solutions in both optically thin and thick regions and the cell size in the optically thick region is not limited by the photon's mean free path.

This paper is organized as follows. Section 2 gives the model equations of radiation transfer equations. Section 3 is the construction of the algorithm on unstructured mesh. Section 4 presents the analysis. In section 5, many numerical tests are included to demonstrate the accuracy and robustness of the new scheme. The last section is the conclusion.

2. System of the gray radiative transfer equations

In this section, we first present the model equations. To simplify the presentation of the scheme on unstructured mesh, the gray radiative transfer equation will be used. The method is general and can be extended directly to more complicated transport equations. The radiative transfer system includes the radiation transport equation and the energy exchange with background material. For the gray approximation, the opacities are independent of the frequency, which can be written in following scaled form:

$$\begin{cases} \dfrac{\epsilon}{c}\dfrac{\partial I}{\partial t} + \vec{\Omega}\cdot\nabla I = \dfrac{\sigma}{\epsilon}\left(\dfrac{1}{4\pi}acT^4 - I\right), \\ \epsilon C_v \dfrac{\partial T}{\partial t} \equiv \epsilon\dfrac{\partial U}{\partial t} = \dfrac{\sigma}{\epsilon}\left(\displaystyle\int I d\vec{\Omega} - acT^4\right). \end{cases} \tag{2.1}$$

Here the spatial variable is denoted by $\vec{r}$, the angular variable is $\vec{\Omega}$, and t is the time variable, $I(\vec{r},\vec{\Omega},t)$ is the radiation intensity, $T(\vec{r},t)$ is the material temperature, $\sigma(\vec{r},T)$ is the opacity, a is the radiation constant, and c is the speed of light, $\epsilon > 0$ is the Knudsen number, and $U(\vec{r},t)$ is the material energy density. For simplicity, the internal source and scattering terms are omitted in (2.1).

Eq. (2.1) is a relaxation model for the radiation intensity to the local thermodynamic equilibrium, in which the emission source is a Planckian at the local material temperature:

$$\frac{1}{4\pi}\sigma acT^4.$$

The material temperature $T(\vec{r},t)$ and the material energy density $U(\vec{r},t)$ are related by

$$\frac{\partial U}{\partial T} = C_V > 0,$$

where $C_V(\vec{r},t)$ is the heat capacity.

As the parameter $\epsilon \to 0$, Larsen et al. [11] had shown that, away from boundaries and initial layers, the intensity I approaches to a Planckian at the local temperature, i.e.,

$$I^{(0)} = \frac{1}{4\pi}ac(T^{(0)})^4,$$

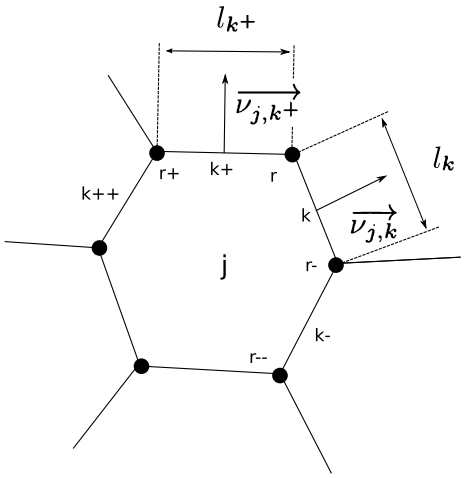

Fig. 1. Unstructured polygonal computational mesh of cell C_j.

and the corresponding local temperature $T^{(0)}$ satisfies the following nonlinear diffusion equation:

$$\frac{\partial}{\partial t}U(T^{(0)}) + a\frac{\partial}{\partial t}(T^{(0)})^4 = \nabla\cdot\frac{ac}{3\sigma}\nabla(T^{(0)})^4. \tag{2.2}$$

In the high opacity region, a preferable multiscale method for the gray radiation transfer equations (2.1) should converge to the diffusion limit (2.2) when ϵ is small and the cell size is not limited by ϵ.

In the following, we will construct such a multiscale method, i.e., the so-called asymptotic preserving implicit UGKS (AP-IUGKS) for (2.1) on unstructured mesh, where the scheme will recover the limiting equation (2.2) automatically. For the angle variable discretization, the discrete ordinate method (DOM) is used. The angle direction is defined as $\vec{\Omega} = (\mu, \xi)$, and $\mu = \sqrt{1-\zeta^2}\cos\theta$, $\xi = \sqrt{1-\zeta^2}\sin\theta$, where $\zeta \in [-1, 1]$ is the cosine value of the angle between the propagation direction $\vec{\Omega}$ and the z-axis, and $\theta \in [0, 2\pi)$ is the angle between the projection vector of $\vec{\Omega}$ onto the xy-plane and the x-axis. Due to the symmetry of angular distribution in a two dimensional case, only the case $\zeta \geq 0$ is considered.

3. AP-IUGKS for system (2.1) on unstructured mesh

In this section, based on the UGKS framework [4], a multi-dimensional AP-IUGKS for the gray radiation transfer system (2.1) on unstructured mesh will be developed.

3.1. The IUGKS for equation (2.1)

Firstly, as a discrete ordinate method for equation (2.1), the propagation direction $\vec{\Omega} = (\mu, \xi)$ is discretized. As introduced in [12] for example, we use the even integer N as the discrete ordinate order, then obtain the discrete directions $\vec{\Omega}_m = (\mu_m, \xi_m)$ and their corresponding integration weights ω_m for $m = 1, \cdots, M$ with $M = N(N+2)/2$. For each direction (μ_m, ξ_m), the discrete equation becomes

$$\begin{cases} \frac{\epsilon}{c}\partial_t I_m + \mu_m\partial_x I_m + \xi_m\partial_y I_m = \frac{\sigma}{\epsilon}(\frac{1}{2\pi}acT^4 - I_m), \\ \epsilon^2 C_v\partial_t T \equiv \epsilon^2\partial_t U = \sigma\Big(\sum_{m=1}^{M} I_m\omega_m - acT^4\Big). \end{cases} \tag{3.1}$$

For the spatial variables, the unstructured mesh in two dimensional case is used, where the computational mesh is assumed to be composed of polygons. For the unstructured mesh, the set of nodes, cells, and edges are denoted by $\mathcal{N}, \mathcal{C}$ and $\mathcal{E}$. In the rest of this paper, the indices j, r, k will be used respectively to specify the cells, nodes, and edges. Fig. 1 shows a 2D polygonal cell 'j' whose area will be denoted by V_j. The cell is defined by the set of nodes $\mathcal{N}(j)$ and the set of edges $\mathcal{E}(j)$. The length of the edge 'k' is denoted by l_k, while $\vec{\nu}_{j,k}$ is the outward normal direction of this edge.

The time is discretized by t^n and the time step is $\Delta t = t^{n+1} - t^n$. For the computational cell C_j, (x_j^c, y_j^c) is the cell center of mass given by

$$\begin{cases} x_j^c = \frac{1}{V_j}\int_{C_j} x dxdy, \\ y_j^c = \frac{1}{V_j}\int_{C_j} y dxdy. \end{cases}$$

Let $I^n_{j,m}$ be the cell averaged value of variable I_m at time t^n in the computational cell C_j, and $\phi(t,x,y) = acT^4$. Then, the integrated equation (3.1) over the cell C_j from time t^n to $t^n + \Delta t$ presents a conservative finite volume scheme

$$\begin{cases} I^{n+1}_{j,m} = I^n_{j,m} - \frac{\Delta t}{V_j} \sum\limits_{k\in\mathcal{E}(j)} F_{j,k,m} + c\Delta t\{\frac{\sigma}{\epsilon^2}(\frac{1}{2\pi}\tilde{\phi}_j - \tilde{I}_{j,m})\}, \\ C_v T^{n+1}_j = C_v T^n_j + \Delta t\{\frac{\sigma}{\epsilon^2}(\sum\limits_{m=1}^{M} \tilde{I}_{j,m}\omega_m - \tilde{\phi}_j)\}, \end{cases} \tag{3.2}$$

where $F_{j,k,m}$ is the time-dependent numerical flux in the outward normal-direction across the cell edge k. The way to construct a time-dependent interface flux plays a dominant role for the multiscale property of UGKS. The terms on the right hand side of (3.2) are given by

$$\begin{aligned} F_{j,k,m} &= \tfrac{c}{\epsilon\Delta t}\int_{t^n}^{t^{n+1}}\int_{k\in\mathcal{E}(j)} \vec{\Omega}_m\cdot\vec{\nu}_{j,k} I_m(t,x,y,\mu_m,\xi_m)dtdS, \quad \forall k\in\mathcal{E}(j), \\ \tilde{\phi}_j &= \tfrac{1}{\Delta t V_j}\int_{t^n}^{t^{n+1}}\int_{C_j}\phi(t,x,y)dxdydt, \\ \tilde{I}_{j,m} &= \tfrac{1}{V_j\Delta t}\int_{t^n}^{t^{n+1}}\int_{C_j} I_m(t,x,y,\mu_m,\xi_m)dxdydt. \end{aligned} \tag{3.3}$$

In order to update the system (3.2), we have to give the explicit formulae for all terms in (3.3). First, the term $\tilde{I}_{j,m}$ in (3.3) can be approximated implicitly by

$$\tilde{I}_{j,m} \approx I^{n+1}_{j,m},$$

which can be combined with the solution on the left hand side of Eq. (3.2).

The following two subsections give the details for the determination of the cell boundary flux $F_{j,k,m}$ and $\tilde{\phi}_j$ in (3.3).

3.2. Cell interface flux in (3.3)

In this subsection, we will give the details of the construction of interface flux $F_{j,k,m}$ for edge $k\in\mathcal{E}(j)$. As shown in the Fig. 1, the middle point of edge k is denoted by $\vec{x}^k_j$ with coordinate $(x^k_j, y^k_j) = ((x(r)+x(r_-))/2.0, (y(r)+y(r_-))/2.0)$. Then, the interface flux is integrated over a time step at the middle point for the total transport

$$\begin{aligned} F_{j,k,m} &= \tfrac{c}{\epsilon\Delta t}\int_{t^n}^{t^{n+1}}\int_{k\in\mathcal{E}(j)} \vec{\Omega}_m\cdot\vec{\nu}_{j,k} I_m(t,x,y,\mu_m,\xi_m)dtdS \\ &\cong \tfrac{cl_k}{\epsilon\Delta t}\int_{t^n}^{t^{n+1}} \vec{\Omega}_m\cdot\vec{\nu}_{j,k} I_m(t,x^k_j,y^k_j,\mu_m,\xi_m)dt. \end{aligned} \tag{3.4}$$

The construction of the time-dependent solution $I_m(t,x^k_j,y^k_j,\mu_m,\xi_m)$ at the middle point (x^k_j,y^k_j) in (3.4) is at the heart of the UGKS approach. The solution is obtained by solving the following initial value problem around the middle point $(x,y) = (x^k_j, y^k_j)$ of the cell interface,

$$\begin{cases} \frac{\epsilon}{c}\partial_t I_m + \mu_m\partial_x I_m + \xi_m\partial_y I_m = \frac{\sigma}{\epsilon}(\frac{1}{2\pi}\bar{\phi} - I_m), \\ I_m(x,y,t)|_{t=t^n} = I_{m,0}(x,y,t^n), \end{cases} \tag{3.5}$$

where the functions $\bar{\phi}(x,y,t)$ and $I_{m,0}(x,y,t^n)$ are reconstructed together with the evolution solution, which will be presented later.

For a unstructured mesh, in order to develop a multi-dimensional scheme, we need consider the flow variation in both normal $\vec{\nu}_{j,k}$ and tangential direction $\vec{T}_{j,k}$. Without loss of generality, the angle between the normal direction $\vec{\nu}_{j,k}$ and the positive global x-coordinate is α with

$$\begin{cases} \vec{\nu}_{j,k} = (\cos\alpha, \sin\alpha), \\ \vec{T}_{j,k} = (-\sin\alpha, \cos\alpha). \end{cases}$$

The coordinate transformation

$$\begin{cases} x' = (x - x^k_j)\cos\alpha + (y - y^k_j)\sin\alpha, \\ y' = -(x - x^k_j)\sin\alpha + (y - y^k_j)\cos\alpha, \end{cases} \tag{3.6}$$

connects the coordinate systems of global $x-y$ and the local orthogonal $x'-y'$. The independent variables in local coordinate system are marked with upper prime script. Then the system (3.5) is changed to

$$\begin{cases} \frac{\epsilon}{c}\partial_t I_m + \mu'_m \partial_{x'} I_m + \xi'_m \partial_{y'} I_m = \frac{\sigma}{\epsilon}(\frac{1}{2\pi}\bar{\phi} - I_m), \\ I_m(x', y', t)|_{t=t^n} = I_{m,0}(x', y', t^n), \end{cases} \tag{3.7}$$

where $\mu'_m = \mu_m \cos\alpha + \xi_m \sin\alpha$ and $\xi'_m = -\mu_m \sin\alpha + \xi_m \cos\alpha$.

After the coordinate transformation (3.6), the middle point (x_j^k, y_j^k) in global coordinate system can be set as the point $(x', y') = (0, 0)$ in the local coordinate system. A time dependent evolution solution for equation (3.7) around the point $(0, 0)$ is given by

$$\begin{aligned} I_m(t, 0, 0, \mu'_m, \xi'_m) = {} & e^{-\vartheta_{j,k}(t-t^n)} I_{m,0}(-\tfrac{c\mu'_m}{\epsilon}(t-t^n), -\tfrac{c\xi'_m}{\epsilon}(t-t^n)) \\ & + \int_{t^n}^{t} e^{-\vartheta_{j,k}(t-s)} \tfrac{c\sigma_{j,k}}{2\pi\epsilon^2} \bar{\phi}(s, -\tfrac{c\mu'_m}{\epsilon}(t-s), -\tfrac{c\xi'_m}{\epsilon}(t-s))ds, \end{aligned} \tag{3.8}$$

where $\vartheta = \frac{c\sigma}{\epsilon^2}$ and $\vartheta_{j,k}$ denotes the corresponding value ϑ at the cell edge, and similarly for $\sigma_{j,k}$.

With the determination of the radiation intensity function I in a local coordinate system (x', y'), the flux across the cell interface can be evaluated by

$$F_{j,k,m} = \frac{cl_k}{\epsilon\Delta t} \int_{t^n}^{t^{n+1}} \mu'_m I_m(t, 0, 0, \mu'_m, \xi'_m)dt. \tag{3.9}$$

Since the velocity has one to one correspondence between the global and local coordinate systems, such as $\mu'_m = \mu_m \cos\alpha + \xi_m \sin\alpha$ and $\xi'_m = -\mu_m \sin\alpha + \xi_m \cos\alpha$, the flux $F_{j,k,m}$ for cell edge $k \in \mathcal{E}(j)$ in (3.3) in the global system can be obtained from the above flux in a local coordinate system.

In order to fully determine the solution in Eq. (3.8), it remains to design an approximation for two unknown functions: the initial state $I_{m,0}(x', y', t^n)$ and the function $\bar{\phi}(t, x', y')$ between the time t^n and t^{n+1} around the middle point $(x', y') = (0, 0)$ in a local coordinate system. Since an implicit scheme is to be developed in this paper for radiative transfer, all above two unknowns will be determined implicitly using iteration, as shown in the next subsection. In the following, the general form of the solution $F_{j,k,m}$ on a unstructured mesh will be presented first.

The initial value function $I_{m,0}(x', y', t^n)$ in (3.5) can be approximated implicitly by a piecewise linear reconstruction function,

$$I_{m,0}(x', y', t^n) = \begin{cases} I_{j,m}^{n+1} + (\delta_{x'} I)_{j,m}^{n+1}(x' - x_j^{c,'}) + (\delta_{y'} I)_{j,m}^{n+1}(y' - y_j^{c,'}), & \text{if } x' < 0, \\ I_{j_1,m}^{n+1} + (\delta_{x'} I)_{j_1,m}^{n+1}(x' - x_{j_1}^{c,'}) + (\delta_{y'} I)_{j_1,m}^{n+1}(y' - y_{j_1}^{c,'}), & \text{if } x' > 0. \end{cases} \tag{3.10}$$

Here the index j_1 denotes the neighboring cell which has the common edge k with cell j. And $(\delta_{x'} I)_{j,m}^{n+1}$, $(\delta_{x'} I)_{j_1,m}^{n+1}$, $(\delta_{y'} I)_{j,m}^{n+1}$, $(\delta_{y'} I)_{j_1,m}^{n+1}$ are the slopes in the local orthogonal coordinate system (x', y') in cells j and j_1 respectively. For the unstructured mesh, these slopes are calculated by a least square method with the implementation of slope limiter for removing the numerical oscillation [14].

For function $\bar{\phi}(x', y', t)$ between t^n and t^{n+1} around the middle point $(0, 0)$, it is expanded at time t^{n+1} implicitly,

$$\bar{\phi}(x', y', t) = \phi_{j,k}^{n+1} + (\delta_t \phi)_{j,k}^{n+1}(t - t^{n+1}) + (\delta_{y'} \phi)_{j,k}^{n+1} y' + \begin{cases} (\delta_{x'} \phi)_{j,k}^{n+1,-} x', & \text{if } x' < 0, \\ (\delta_{x'} \phi)_{j_1,k}^{n+1,+} x', & \text{if } x' > 0. \end{cases} \tag{3.11}$$

Here $\phi_{j,k}^{n+1}$ is the value to be determined.

In order to give the explicit formula of the derivatives in (3.11), we first define the values of ϕ on node r and r_-

$$\begin{cases} \hat{\phi}_r^{n+1} = (\sum_{j \in \mathcal{C}(r)} \phi_j^{n+1})/N_r^c, \\ \hat{\phi}_{r_-}^{n+1} = (\sum_{j \in \mathcal{C}(r_-)} \phi_j^{n+1})/N_{r_-}^c, \end{cases}$$

where $\mathcal{C}(r)$ is the set of cells which have the common node r, and N_r^c is the corresponding number of the set $\mathcal{C}(r)$. Similarly, $\mathcal{C}(r_-)$ and $N_{r_-}^c$ can be defined. The one-sided slopes in (3.11) are given by

$$\begin{aligned} (\delta_{x'} \phi)_{j,k}^{n+1,-} &= \frac{1}{L_{j,k}^-}(\phi_{j,k}^{n+1} - \phi_j^{n+1} - \tau_{j,k}^-(\hat{\phi}_r^{n+1} - \hat{\phi}_{r_-}^{n+1})), \\ (\delta_{x'} \phi)_{j,k}^{n+1,+} &= -\frac{1}{L_{j,k}^+}(\phi_{j,k}^{n+1} - \phi_{j_1}^{n+1} - \tau_{j,k}^+(\hat{\phi}_{r_-}^{n+1} - \hat{\phi}_r^{n+1})), \end{aligned} \tag{3.12}$$

where $L^-_{j,k}, L^+_{j,k}, \tau^-_{j,k}, \tau^+_{j,k}$ are the projected lengths given by

$$\begin{cases} L^-_{j,k} = (x^k_j - x^c_j, y^k_j - y^c_j)\cdot \vec{e}_{x'}, \\ L^+_{j,k} = -(x^k_j - x^c_{j_1}, y^k_j - y^c_{j_1})\cdot \vec{e}_{x'}, \\ \tau^-_{j,k} = \frac{(x^k_j - x^c_j, y^k_j - y^c_j)\cdot \vec{e}_{y'}}{l_k}, \\ \tau^+_{j,k} = -\frac{(x^k_j - x^c_{j_1}, y^k_j - y^c_{j_1})\cdot \vec{e}_{y'}}{l_k}. \end{cases}$$

In fact, the derivatives $(\delta_{x'}\phi)^{n+1,-}_{j,k}, (\delta_{x'}\phi)^{n+1,+}_{j,k}$ in (3.12) are equal to the normal derivatives in a global $x-y$ coordinate system at the edge, which can be obtained by the following way. Let $\vec{\gamma}_1, \vec{\gamma}_2$ be two unit vectors given by

$$\vec{\gamma}_1 = \frac{(x^k_j - x^c_j, y^k_j - y^c_j)}{|(x^k_j - x^c_j, y^k_j - y^c_j)|}, \quad \vec{\gamma}_2 = \frac{(x(r) - x(r_-), y(r) - y(r_-))}{|(x(r) - x(r_-), y(r) - y(r_-))|},$$

and let the angle between the vector $\vec{\gamma}_1$ and the edge normal vector $\vec{\nu}_{j,k}$ be θ^k_j, then we have

$$\vec{\nu}_{j,k} = -\tan\theta^k_j \vec{\gamma}_2 + \frac{1}{\cos\theta^k_j}\vec{\gamma}_1,$$

and

$$(\delta_{x'}\phi)^{n+1,-}_{j,k} = \nabla\phi\cdot\vec{\nu}_{j,k} = \nabla\phi\cdot(-\tan\theta^k_j\vec{\gamma}_2 + \tfrac{1}{\cos\theta^k_j}\vec{\gamma}_1). \tag{3.13}$$

Furthermore, if we take the direction-derivatives in (3.13) as the following formula

$$\nabla\phi\cdot\vec{\gamma}_1 = \frac{\phi^{n+1}_{j,k} - \phi^{n+1}_j}{|(x^k_j - x^c_j, y^k_j - y^c_j)|},$$
$$\nabla\phi\cdot\vec{\gamma}_2 = \frac{\hat{\phi}^{n+1}_r - \hat{\phi}^{n+1}_{r_-}}{|(x(r) - x(r_-), y(r) - y(r_-))|},$$

we obtain the first equation of (3.12). The second equation of (3.12) is the outward normal derivative of the cell j_0, which can be obtained similarly.

The time derivative $(\delta_t\phi)^{n+1}_{i+1/2,j}$ is discretized by

$$(\delta_t\phi)^{n+1}_{j,k} = \frac{\phi^{n+1}_{j,k} - \phi^n_{j,k}}{\Delta t}.$$

The derivative $(\delta_{y'}\phi)^{n+1}_{j,k}$ is

$$(\delta_{y'}\phi)^{n+1}_{j,k} = \frac{\hat{\phi}^{n+1}_r - \hat{\phi}^{n+1}_{r_-}}{l_k}.$$

The cell boundary value $\phi^{n+1}_{j,k}$ and the cell center value $\phi^{n+1}_j, \phi^{n+1}_{j_0}$ in the above equations will be evaluated in the next subsection through an implicit solver for macroscopic equations.

Based on the above modeling, the numerical flux

$$F_{j,k,m} = \frac{cl_k}{\epsilon\Delta t}\int_{t^n}^{t^{n+1}} \mu'_m I_m(t,0,0,\mu'_m,\xi'_m)dt$$

can be exactly evaluated by using the expressions (3.8), (3.10) and (3.11),

$$\begin{aligned} F_{j,k,m} = l_k\{ & A_{j,k}\mu'_m(I^{-,'}_{j,k,m}1_{\mu'_m>0} + I^{+,'}_{j,k,m}1_{\mu'_m<0}) \\ & + C_{j,k}\mu'_m\phi^{n+1}_{j,k} \\ & + D_{j,k}[(\mu'_m)^2((\delta_{x'}\phi)^{n+1,-}_{j,k}1_{\mu'_m>0} + (\delta_{x'}\phi)^{n+1,+}_{j,k}1_{\mu'_m<0}) + \mu'_m\xi'_m(\delta_{y'}\phi)^{n+1}_{j,k}] \\ & + B_{j,k}([(\mu'_m)^2(\delta_{x'}I)^{n+1}_{j,m} + \mu'_m\xi'_m(\delta_{y'}I)^{n+1}_{j,m}]1_{\mu'_m>0} + [(\mu'_m)^2(\delta_{x'}I)^{n+1}_{j_1,m} + \mu'_m\xi'_m(\delta_{y'}I)^{n+1}_{j_1,m}]1_{\mu'_m<0}) \\ & + E_{j,k}\mu'_m(\delta_t\phi)^{n+1}_{j,k}\}, \end{aligned} \tag{3.14}$$

where $I^{-,'}_{j,k,m}, I^{+,'}_{j,k,m}$ are the boundary values

$$I^{-,'}_{j,k,m} = I^{n+1}_{j,m} + (\delta_{x'} I)^{n+1}_{j,m}(-x^{c,'}_j) + (\delta_{y'} I)^{n+1}_{j,m}(-y^{c,'}_j),$$
$$I^{+,'}_{j,k,m} = I^{n+1}_{j_1,m} + (\delta_{x'} I)^{n+1}_{j_1,m}(-x^{c,'}_{j_1}) + (\delta_{y'} I)^{n+1}_{j_1,m}(-y^{c,'}_{j_1}),$$

and the coefficients in (3.14) are given by

$$\begin{aligned}
A(\Delta t,\epsilon,\sigma,\vartheta) &= \tfrac{c}{\epsilon\Delta t\vartheta}(1-e^{-\vartheta\Delta t}),\\
C(\Delta t,\epsilon,\sigma,\vartheta) &= \tfrac{c^2\sigma}{2\pi\Delta t\epsilon^3\vartheta}(\Delta t - \tfrac{1}{\vartheta}(1-e^{-\vartheta\Delta t})),\\
D(\Delta t,\epsilon,\sigma,\vartheta) &= -\tfrac{c^3\sigma}{2\pi\Delta t\epsilon^4\vartheta^2}(\Delta t(1+e^{-\vartheta\Delta t}) - \tfrac{2}{\vartheta}(1-e^{-\vartheta\Delta t})),\\
B(\Delta t,\epsilon,\sigma,\vartheta) &= -\tfrac{c^2}{\epsilon^2\vartheta^2\Delta t}(1-e^{-\vartheta\Delta t} - \vartheta\Delta t e^{-\vartheta\Delta t}),\\
E(\Delta t,\epsilon,\sigma,\vartheta) &= \tfrac{c^2\sigma}{2\pi\epsilon^3\vartheta^3\Delta t}(1-e^{-\vartheta\Delta t} - \vartheta\Delta t e^{-\vartheta\Delta t} - \tfrac{1}{2}(\vartheta\Delta t)^2),
\end{aligned} \tag{3.15}$$

with $\vartheta = \frac{c\sigma}{\epsilon^2}$.

The expressions (3.15) have the following functional dependence,

$$\begin{aligned}
A_{j,k} &= A(\Delta t,\epsilon,\sigma^{n+1}_{j,k},\vartheta^{n+1}_{j,k}),\\
C_{j,k} &= C(\Delta t,\epsilon,\sigma^{n+1}_{j,k},\vartheta^{n+1}_{j,k}),\\
D_{j,k} &= D(\Delta t,\epsilon,\sigma^{n+1}_{j,k},\vartheta^{n+1}_{j,k}),\\
B_{j,k} &= B(\Delta t,\epsilon,\sigma^{n+1}_{j,k},\vartheta^{n+1}_{j,k}),\\
E_{j,k} &= E(\Delta t,\epsilon,\sigma^{n+1}_{j,k},\vartheta^{n+1}_{j,k}).
\end{aligned} \tag{3.16}$$

The multiscale nature of UGKS depends on the limiting values of the above coefficients. Even with the general interface solution (3.8), in order to obtain a consistent diffusion limit flux, the coefficients, such as σ, at a cell edge k, have to be properly defined by using the values from two neighboring cells j and j_1 in (3.16). The details procedure of the derivation of expressions (3.14) to (3.16) is given in Appendix A. Up to now, a complete description of the numerical cell interface flux for equation (3.1) is presented with the unknown macro-quantities in (3.14), which will be determined in the next subsection.

3.3. IUGKS

3.3.1. Update of radiation energy and temperature

To complete the construction of numerical scheme for (3.2), the detailed expressions $\bar{\phi}$ in (3.5), and especially $\phi^{n+1}_{j,k}$, ϕ^{n+1}_j, and $\phi^{n+1}_{j_1}$ in (3.11), have to be determined. Following the UGKS framework, the macroscopic radiation energy and material temperature equations will be solved numerically first. Let's take the angular integration on the first equation in (2.1) and obtain the following system for macroscopic variables:

$$\begin{cases}
\dfrac{\epsilon^2}{c}\dfrac{\partial\rho}{\partial t} + \epsilon\nabla\cdot <\vec{\Omega}I> = \sigma(\phi-\rho),\\
\epsilon^2 C_v\dfrac{\partial T}{\partial t} \equiv \epsilon^2\dfrac{\partial U}{\partial t} = \sigma(\rho-\phi),
\end{cases} \tag{3.17}$$

where $\phi = acT^4$, $\rho = \int_{4\pi} Id\vec{\Omega}$, and $<\vec{\Omega}I>$ is the angular vector integration given by

$$<\vec{\Omega}I> = \int_{4\pi}\vec{\Omega}Id\vec{\Omega}.$$

In order to obtain the macro-quantities ρ and ϕ at the next time level through the above equation (3.17), let's first define an exact relationship between the material energy density U and the radiation energy density $\phi = acT^4$ by

$$\beta(x,t) = \frac{\partial\phi}{\partial U} = \frac{d\phi}{dT}\frac{dT}{dU} = \frac{4acT^3}{C_v(T)}. \tag{3.18}$$

Then the system (3.17) can be rewritten as

$$\begin{cases}
\dfrac{\epsilon^2}{c}\dfrac{\partial\rho}{\partial t} + \epsilon\nabla\cdot <\vec{\Omega}I> = \sigma(\phi-\rho),\\
\epsilon^2\dfrac{\partial\phi}{\partial t} = \beta\sigma(\rho-\phi).
\end{cases} \tag{3.19}$$

The numerical discretization for the above macroscopic equations (3.17) can be written as

$$\begin{cases} \rho_j^{n+1} = \rho_j^n - \frac{\Delta t}{V_j} \sum_{k\in\mathcal{E}(j)} \Phi_{j,k}^{n+1} + \dfrac{c\Delta t \sigma_j^{n+1}}{\epsilon^2}(\phi_j^{n+1} - \rho_j^{n+1}), \\ \phi_j^{n+1} = \phi_j^n + \frac{(\beta\sigma)_j^{n+1}\Delta t}{\epsilon^2}(\rho_j^{n+1} - \phi_j^{n+1}), \end{cases} \tag{3.20}$$

where the cell interface fluxes are given by

$$\Phi_{j,k}^{n+1} = \frac{cl_k}{\epsilon\Delta t}\int_{t^n}^{t^n+\Delta t} \vec{v}_{j,k}\cdot < \vec{\Omega} I > (x_j^k, y_j^k, t)dt, \quad \forall k \in \mathcal{E}(j), \tag{3.21}$$

where (x_j^k, y_j^k) is the coordinate of the middle point of edge k.

With the cell interface intensity I in (3.8), we can get the explicit expression for all terms in (3.21). For example, for edge k, we can get

$$\begin{aligned} \Phi_{j,k}^{n+1} &= \frac{cl_k}{\epsilon\Delta t}\int_{t^n}^{t^n+\Delta t} \vec{v}_{j,k}\cdot < \vec{\Omega} I > (x_j^k, y_j^k, t)dt \\ &= l_k \sum_{m=1}^{M} \omega_m F_{j,k,m} \\ &= l_k\{A_{j,k}^{n+1}\sum_{m=1}^{M}\omega_m\mu_m'(I_{j,k,m}^{-,'}1_{\mu_m'>0} + I_{j,k,m}^{+,'}1_{\mu_m'<0}) + \\ &\quad \frac{\pi D_{j,k}^{n+1}}{3}((\delta_{x'}\phi)_{j,k}^{n+1,-} + (\delta_{x'}\phi)_{j,k}^{n+1,+}) + \\ &\quad B_{j,k}^{n+1}\sum_{m=1}^{M}\omega_m(\mu_m')^2((\delta_{x'}I)_{j,m}^{n+1}1_{\mu_m'>0} + (\delta_{x'}I)_{j_1,m}^{n+1}1_{\mu_m'<0})\}, \end{aligned} \tag{3.22}$$

where the expression of $A_{j,k}^{n+1}$, $B_{j,k}^{n+1}$ and $D_{j,k}^{n+1}$ in (3.22) are the same as the parameters $A_{j,k}$, $B_{j,k}$, and $D_{j,k}$ in (3.16), but with the following definitions for the cell interface values $\sigma_{j,k}^{n+1}$,

$$\sigma_{j,k}^{n+1} = \frac{2\sigma_j^{n+1}\sigma_{j_1}^{n+1}}{\sigma_j^{n+1}+\sigma_{j_1}^{n+1}}. \tag{3.23}$$

The macro-boundary flux $\Phi_{j,k}^{n+1}$ depends on the cell values $\phi_j^{n+1}, \phi_{j_1}^{n+1}$, and boundary value $\phi_{j,k}^{n+1}$ due to determination of the derivatives $(\delta_{x'}\phi)_{j,k}^{n+1,-}$ and $(\delta_{x'}\phi)_{j,k}^{n+1,+}$. With the assumption of a continuous normal derivative, we set the relation

$$(\delta_{x'}\phi)_{j,k}^{n+1,-} = (\delta_{x'}\phi)_{j,k}^{n+1,+}.$$

Then, we have

$$\begin{aligned} \phi_{j,k}^{n+1} &= \frac{[L_{j,k}^-\phi_{j_1}^{n+1} + L_{j,k}^+\phi_j^{n+1} + (L_{j,k}^-\tau_{j,k}^+ - L_{j,k}^+\tau_{j,k}^-)(\hat{\phi}_{r_-}^{n+1} - \hat{\phi}_r^{n+1})]}{L_{j,k}^- + L_{j,k}^+}, \\ (\delta_{x'}\phi)_{j,k}^{n+1,-} &= K_{j,k}(\phi_{j_1}^{n+1} - \phi_j^{n+1} - \tau_{j,k}(\hat{\phi}_r^{n+1} - \hat{\phi}_{r_-}^{n+1})), \end{aligned} \tag{3.24}$$

where $K_{j,k} = \frac{1}{L_{j,k}^- + L_{j,k}^+}$, $\tau_{j,k} = \tau_{j,k}^- + \tau_{j,k}^+ = \frac{(x_{j_1}^c - x_j^c, y_{j_1}^c - y_j^c)\cdot\vec{e}_{y'}}{l_k}$.

Up to now, with the given interface fluxes in (3.21), the equations (3.20) become a coupled nonlinear system for the macroscopic quantities ϕ_j^{n+1} and ρ_j^{n+1}, where the parameters σ_j^{n+1} and β_j^{n+1} depend implicitly on the material temperature T_j^{n+1}. This nonlinear system can be solved by an iterative method.

After obtaining T_j^{n+1} in the macroscopic variable equations (3.17), we get ϕ_j^{n+1}. Then, $\tilde{\phi}_j$ in (3.2) is set by

$$\tilde{\phi}_j = \phi_j^{n+1}, \tag{3.25}$$

and the cell interface value $\phi_{j,k}^{n+1}$ in (3.14) takes

$$\phi_{j,k}^{n+1} = \frac{\left[L_{j,k}^-\phi_{j_1}^{n+1} + L_{j,k}^+\phi_j^{n+1} + (L_{j,k}^-\tau_{j,k}^+ - L_{j,k}^+\tau_{j,k}^-)(\hat{\phi}_{r_-}^{n+1} - \hat{\phi}_r^{n+1})\right]}{L_{j,k}^- + L_{j,k}^+}. \tag{3.26}$$

The cell interface opacities $\sigma_{j,k}$ and $\vartheta_{j,k}$ are re-evaluated with the above updated material temperature T_j^{n+1} from the converged macroscopic solutions (3.17). As a result, the boundary flux $F_{j,k,m}$ in (3.14) for the micro equation (3.2) can be evaluated again, which is fully determined. In the following, we give the update of microscopic variables in (3.2).

3.3.2. Update of radiation intensity and material temperature

After the determination of macroscopic material energy ϕ_j^{n+1} and material temperature T_j^{n+1} above, the interface flux function for the radiation intensity of the system (3.3) can be obtained. The radiative transfer equation in (3.2) can be solved by the following scheme

$$I_{j,m}^{n+1} = I_{j,m}^{n} - \frac{\Delta t}{V_j}\sum_{k\in\mathcal{E}(j)} F_{j,k,m} + \frac{c\Delta t\sigma_j^{n+1}}{\epsilon^2}\left(\frac{1}{2\pi}\phi_j^{n+1} - I_{j,m}^{n+1}\right), \tag{3.27}$$

where the opacity σ_j^{n+1} is defined by the updated material temperature T_j^{n+1} of the macro equations (3.17).

The final step is to solve the second equation of (3.2) to obtain the final material temperature with the newly updated value $I_{j,m}^{n+1}$. This material energy is directly given by

$$\phi_j^{n+1} = \frac{\phi_j^n + \Delta t(\beta\sigma)_j^{n+1}\sum_{m=1}^{M}\omega_m I_{j,m}^{n+1}/\epsilon^2}{1 + \Delta t(\beta\sigma)_j^{n+1}/\epsilon^2}. \tag{3.28}$$

Based on (3.28), we immediately obtain the material temperature $T_j^{n+1} = (\phi_j^{n+1}/(ac))^{1/4}$.

This completes the construction of the IUGKS for the gray radiative transfer equations (2.1) on unstructured mesh. Since the flux $F_{j,k,m}$ in (3.27) is implicitly dependent on the solution of radiation intensity, the solutions of (3.27) and (3.28) are updated with the coupling of the macro-solver of (3.20). The whole procedure is solved through an iteration process. The numerical steps of IUGKS is summarized in the following.

3.3.3. Overall numerical procedure

Loop of the IUGKS: To solve the equation (3.2). First for given $I_{j,m}^n$ and T_j^n at time step n, then evaluate ρ_j^n and ϕ_j^n, and find $I_{j,m}^{n+1}$ and T_j^{n+1} at time step $n+1$.

1) Let $T^{n+1,0} = T^n$, $I_{j,m}^{n+1,0} = I_{j,m}^n$;
2) For $s = 1, \cdots, S$
{
2.1) With $I_{j,m}^{n+1} = I_{j,m}^{n+1,s-1}$ in equation (3.21). Solve the system (3.20) by *iteration method* to obtain ϕ_j^{n+1} and ρ_j^{n+1}, then T_j^{n+1};
2.2) Use the obtained values T_j^{n+1} and ϕ_j^{n+1} from the above step, to solve the resulting implicit equation (3.27) by *iteration method* to get $I_{j,m}^{n+1}$;
2.3) Based on the solution $I_{j,m}^{n+1}$, to get the new value ϕ_j^{n+1} by using the explicit expression (3.28), then get the material temperature T_j^{n+1};
2.4) Set $I_{j,m}^{n+1,s} = I_{j,m}^{n+1}$, $T_j^{n+1,s} = T_j^{n+1}$;
2.5) Calculate the iteration error, exit if convergence.
}
3) Set the final solution at time t^{n+1} by $I_{j,m}^{n+1} = I_{j,m}^{n+1,s}$, $T_j^{n+1} = T_j^{n+1,s}$;
4) Set the initial data value for next computational step by $I_{j,m}^n = I_{j,m}^{n+1}$, $T_j^n = T_j^{n+1}$.

It should be pointed out that in the above algorithm of IUGKS, the steps 2.1) and 2.2) need to be solved by iterative method for the resulting implicit system. In this paper, these two equations are solved by the simple Gauss–Seidel iteration technique.

In the following section, we will present the asymptotic analysis of the above scheme and show that the scheme solves the diffusion equations in the optically thick region automatically.

4. Asymptotic analysis of IUGKS on unstructured mesh

In this section, we shall analyze the asymptotic properties of the IUGKS for radiative transfer system. The methods in [1,13] will be used for the analysis. The property of the scheme is mainly determined by the numerical flux, which is controlled through the ϵ-dependent coefficients in (3.15) and (3.16). These coefficient satisfy the following Proposition 1.

Proposition 1. *Let the opacity coefficient σ be positive. Then as ϵ tends to zero, we have*

- $A(\Delta t, \epsilon, \sigma, \vartheta)$ *tends to 0;*
- $B(\Delta t, \epsilon, \sigma, \vartheta)$ *tends to 0;*
- $D(\Delta t, \epsilon, \sigma, \vartheta)$ *tends to* $-c/(2\pi\sigma)$.

Thus, the corresponding macroscopic diffusion flux $(\text{Diff})_{j,k}^{n+1}$, defined by

$$\begin{aligned}(\text{Diff})_{j,k}^{n+1} &= < \tfrac{c\vec{\Omega}\cdot\vec{\nu}_{j,k}}{\epsilon\Delta t}\int_{t^n}^{t^{n+1}} I(t, x_j^k, y_j^k, \mu, \xi)dt > \\ &= \int_{2\pi} \tfrac{c\vec{\Omega}\cdot\vec{\nu}_{j,k}}{\epsilon\Delta t}\int_{t^n}^{t^{n+1}} I(t, x_j^k, y_j^k, \mu, \xi)dtd\mu d\xi \\ &= \int_{2\pi} \tfrac{c\mu'}{\epsilon\Delta t}\int_{t^n}^{t^{n+1}} I(t, 0, 0, \mu', \xi')dtd\mu' d\xi',\end{aligned} \tag{4.1}$$

has the limiting solution

$$\begin{aligned}(\text{Diff})_{j,k}^{n+1} &= \sum_{m=1}^{M}\omega_m\mu_m' I_m(t, 0, 0, \mu_m', \xi_m') \\ \xrightarrow[\epsilon\to 0]{} &-(\tfrac{c}{6\sigma_{j,k}}(\delta_{x'}\phi)_{j,k}^{n+1,-} + \tfrac{c}{6\sigma_{j,k}}(\delta_{x'}\phi)_{j,k}^{n+1,+}) \\ &= -\tfrac{c}{3\sigma_{j,k}}\{K_{j,k}(\phi_{j_1}^{n+1} - \phi_j^{n+1} - \tau_{j,k}(\hat{\phi}_r^{n+1} - \hat{\phi}_{r_-}^{n+1}))\}.\end{aligned} \tag{4.2}$$

For the non-orthogonal mesh, $\tau_{j,k} \neq 0$, this limiting solution (4.2), which depends on the cell values $\phi_{j_1}^{n+1}, \phi_j^{n+1}$ and node values $\hat{\phi}_r^{n+1}, \hat{\phi}_{r_-}^{n+1}$, gives the numerical flux of an asymptotic diffusion equation on unstructured mesh.

With the Proposition 1 and the relation (4.2), it can be shown that the lUGKS is an asymptotic preserving method through the following Proposition 2.

Proposition 2. *Let parameter σ be positive. Then, as ϵ tends to zero, the numerical scheme given by (3.20), (3.27), and (3.28) approaches to the implicit scheme for the diffusion limit equation (2.2) on unstructured mesh, which reduces to the standard implicit nine points diffusion scheme in two dimensional distorted quadrilateral mesh, and to the standard five points scheme for two-dimensional rectangular orthogonal mesh.*

Proof. Firstly, on the order of ϵ^{-2} in (3.27), as the parameter ϵ tends to zero, we have

$$I_{j,m}^{n+1} \to \frac{1}{2\pi}\phi_j^{n+1}.$$

Multiplying the above equation with integration weighting function ω_m and summing the resulting equation over the angle variable, then as $\epsilon \to 0$, we have

$$\rho_j^{n+1} \to \phi_j^{n+1}. \tag{4.3}$$

Secondly, on the order of ϵ^{-1} in (3.27), such as the flux $F_{j,k,m}^{n+1}$ given by (3.14), the macro flux $\Phi_{j,k}^{n+1}$ in equation (3.22) can be obtained by multiplying the flux $F_{j,k,m}^{n+1}$ with the integration weight ω_m and summing over the angle variable. By Proposition 1, as $\epsilon \to 0$ we get

$$\Phi_{j,k}^{n+1} \to -\frac{cl_k}{3\sigma_{j,k}^{n+1}}\big[K_{j,k}(\phi_{j_1}^{n+1} - \phi_j^{n+1} - \tau_{j,k}(\hat{\phi}_{j,r}^{n+1} - \hat{\phi}_{j,r_-}^{n+1}))\big]. \tag{4.4}$$

Thirdly, multiplying the integration weight ω_m to equation (3.27) and summing over the angle variable, as the parameter $\epsilon \to 0$, we have

$$\begin{aligned}\rho_j^{n+1} = \rho_j^n - \tfrac{\Delta t}{V_j}\sum_{k\in\mathcal{E}(j)}\{-\frac{cl_k}{3\sigma_{j,k}}\big[K_{j,k}(\phi_{j_1}^{n+1} - \phi_j^{n+1} - \tau_{j,k}(\hat{\phi}_{j,r}^{n+1} - \hat{\phi}_{j,r_-}^{n+1}))\big]\} + \\ c\Delta t\sum_{m=1}^{M}\omega_m\sigma_j^{n+1}(I_{j,m}^{n+1} - \frac{1}{2\pi}\phi_j^{n+1})/\epsilon^2.\end{aligned} \tag{4.5}$$

The combination of the two equations (4.5) and (3.28) gives

$$\rho_{i,j}^{n+1} = \rho_{i,j}^n + \tfrac{\Delta t}{V_j}\sum_{k\in\mathcal{E}(j)}\{\frac{cl_k}{3\sigma_{j,k}}\big[K_{j,k}(\phi_{j_1}^{n+1} - \phi_j^{n+1} - \tau_{j,k}(\hat{\phi}_{j,r}^{n+1} - \hat{\phi}_{j,r_-}^{n+1}))\big]\} - cC_v(T_j^{n+1} - T_j^n). \tag{4.6}$$

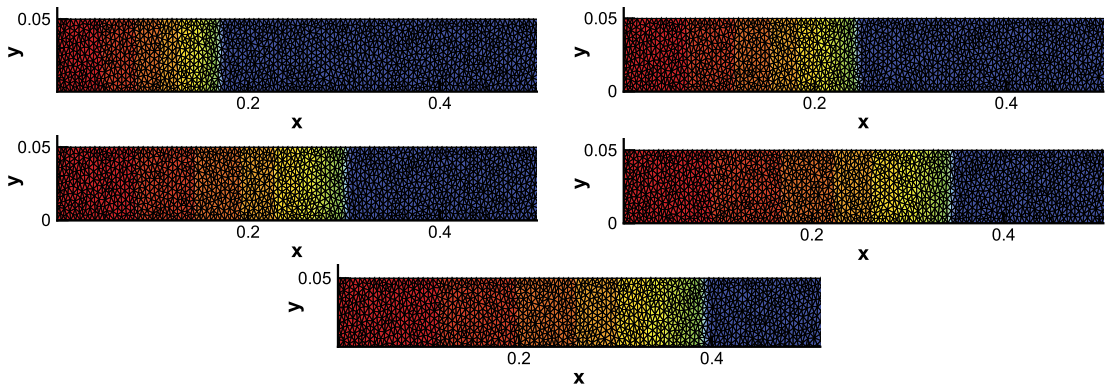

Fig. 2. The contour of material temperature for Marshak wave-2B problem at times 15 ns, 30 ns, 45 ns, 60 ns and 74 ns from top to bottom respectively.

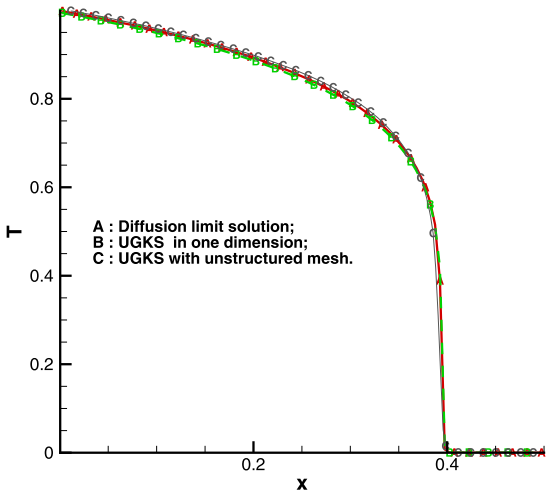

Fig. 3. The material temperature comparison with the result of [1] and the diffusion limit solution for Marshak wave-2B problem at time 74 ns.

As a result, equation (4.6) is a scheme for diffusion equation (2.2) on unstructured mesh. For non-orthogonal mesh, i.e., $\tau_{j,k} \neq 0$, based on the construction of node values $\hat{\phi}^{n+1}_{j,r}$ and $\hat{\phi}^{n+1}_{j,r_-}$, it is clear that the scheme (4.6) becomes a standard nine points scheme for diffusion equation on distorted quadrilateral mesh. The scheme can be further reduced to the standard five points method for orthogonal quadrilateral mesh, see [17] for the direct construction of such a scheme from diffusion equation. This shows that the current scheme for gray radiative transfer equations (2.1) on unstructured mesh is an asymptotic preserving method. □

The benefit for the construction of IUGKS is not only for the recovery of kinetic and diffusive limiting solutions. Actually, accurate solutions can be obtained from UGKS in the whole transition regime with a changeable value of ϵ.

5. Numerical tests

In the following, we simulate gray radiative transfer problems in two-dimensional unstructured and distorted quadrilateral mesh. In the computations, the unit of length is taken to be centimeter (cm), the mass unit is gram (g), the time unit is nanosecond (ns), the temperature unit is kilo electronvolt (keV), and the energy unit is 10^9 Joules (GJ). And under the above units, the speed of light is 29.98 cm/ns and the radiation constant a is 0.01372 GJ/(cm^3 $*$ keV^4). Since the implicit method is used, the CFL condition is released in the following simulations.

Example 1 *(Marshak wave-2B).* In this example we take the absorption/emission coefficient to be $\sigma = 100/T^3$ cm^2/g, the specific heat to be 0.1 GJ/g/keV, and the density to be 3.0 g/cm^3. The initial material temperature T is set to be 10^{-6} keV. The computational domain is a two-dimensional unstructured mesh with 821 nodes and 1236 cells. As a boundary condition, a constant isotropic incident radiation with a Planckian distribution and intensity 1 keV is kept on the left boundary. In Fig. 2 the computed radiation wave fronts at times 15, 30, 45, 60 and 74 ns are given. By comparing with the result of [1] in Fig. 3, we can see that the computed material temperature for gray radiation transfer equation agree very well

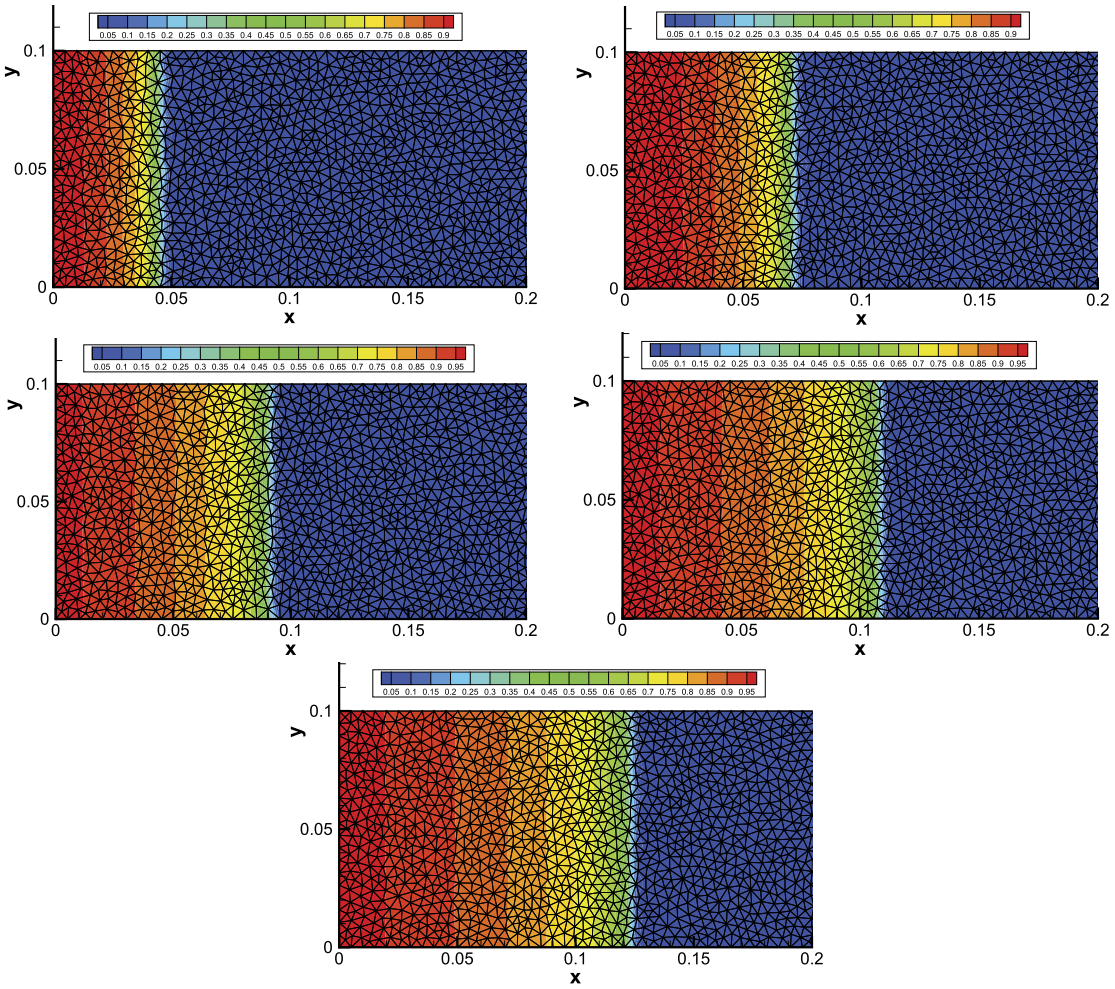

Fig. 4. The contour of the material temperature for Marshak wave-2A problem at times 0.2 ns, 0.4 ns, 0.6 ns, 0.8 ns and 1 ns respectively.

with the result of diffusion limiting solution at time 74 ns. It shows that with large absorption/emission coefficient, the results converge to the diffusive limiting solutions.

Example 2 *(Marshak wave-2A).* The Marshak wave-2A problem is exactly the same as the Marshak wave-2B problem except that it has an absorption/emission coefficient $\sigma = 10/T^3$ cm^2/g. For this case, the computational domain is a two-dimensional unstructured mesh with 5844 nodes and 11250 cells. It turns out that the small absorption/emission coefficient violates the equilibrium diffusion approximation. The IUGKS also works well for this problem. In Fig. 4, the numerical results of the radiation wave front at times 0.2, 0.4, 0.6, 0.8, 1.0 ns are shown. By comparing with the result of [1] in Fig. 5, it shows that with a small absorption/emission coefficient the IUGKS gives quite different solutions from the diffusion equation results.

Example 3. This problem is the combing of Marshak wave-2A problem and the Marshak wave-2B problem. The absorption/emission coefficient is given by

$$\sigma = \begin{cases} 100/T^3 \text{ cm}^2/\text{g}, & \text{for } x \le 0.4; \\ 0.1/T^3 \text{ cm}^2/\text{g}, & \text{otherwise.} \end{cases}$$

And the initial material temperature T is set to be

$$T = \begin{cases} 1 \text{ keV}, & \text{for } 0.3 \le x \le 0.4; \\ 10^{-6} \text{ keV}, & \text{otherwise.} \end{cases}$$

For this case, the computational domain is a two-dimensional unstructured mesh with 5844 nodes and 11250 cells. In Fig. 6, the numerical results of the radiation wave front at times 20 ns are shown. By comparing with the result with the

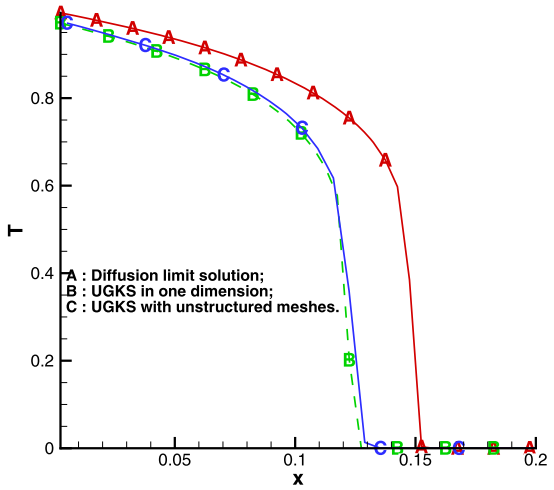

Fig. 5. The material temperature comparison with the result of [1] and the diffusion limit solution for Marshak wave-2A problem at time 1 ns.

equilibrium diffusion approximation, the UGKS solution is very close to the diffusive limit result in the optically thick region. But, they are different in the optically thin region.

Example 4 *(Tophat test [3]).* This is a 2D problem. The size of the simulation domain is $[0, 7] \times [-2, 2]$. Dense, opaque material with density 10 g/cm^3, and opacity $\sigma = 2000$ cm^{-1} is located in the following regions: $(3, 4) \times (-1, 1)$, $(0, 2.5) \times (-2, -0.5)$, $(0, 2.5) \times (0.5, 2)$, $(4.5, 7) \times (-2, -0.5)$, $(4.5, 7) \times (0.5, 2)$, $(2.5, 4.5) \times (-2, -1.5)$, $(2.5, 4.5) \times (1.5, 2.0)$. The pipe, with density 0.01 g/cm^3 and opacity $\sigma = 0.2$ cm^{-1}, occupies all other regions. The heat capacity for unit mass is 0.1 GJ/g/keV. Initially, the material has a temperature 0.05 keV everywhere, and the radiation and material temperature are in equilibrium. A heating source with a fixed temperature 0.5 keV is located on the left boundary for $-0.5 < y < 0.5$. All the other boundary conditions are outflow. Five probes are placed at $(x = 0.25, y = 0)$, $(x = 2.75, y = 0)$, $(x = 3.5, y = 1.25)$, $(x = 4.25, y = 0)$, and $(x = 6.75, y = 0)$ to monitor the change of the temperature in the thin opacity region. We simulate this problem with unstructured mesh both in optically thin and optically thick region. The mesh has 4484 nodes and 8746 cells, which is given in Fig. 7. We show the contours of the material temperature and radiation temperature at three times 8 ns, 94 ns and 1000 ns respectively in Fig. 8. In comparison with the results of [3], the interface between the optically thick and thin materials is captured sharply by IUGKS method. In Fig. 9, the time evolution of the material and radiation temperature at five probe points are given. Since the outflow condition is used at the right boundary, at the fifth probe point it shows that the temperature cools off slightly before being heated up by the radiation wave, which has agreement with the observation in [3] and [1].

6. Conclusion

In this paper, we present an implicit unified gas kinetic scheme for the gray radiative transfer equations on unstructured mesh to deal with the complex geometry. For the implicit method, the CFL constraint for the time step is not needed any more, so a large time step can be used in numerical simulation. As a result, the computational efficiency is much improved. This also paves the way to connect the schemes for the radiative transfer equation and the hydrodynamical ones, where a large time step is usually used due to the limited fluid velocity in comparison with the speed of light. Another improvement of IUGKS from the former schemes [1,16] on the uniform structured mesh is the construction of the interface flux function. In this paper, for the first time on unstructured mesh a multi-dimensional flux function is constructed, where the time evolution of the radiation intensity at a cell interface includes the contributions of radiative gradients in both normal and tangential directions. Only under such a construction, a full diffusion equation can be properly discretized on unstructured mesh in the diffusive limit. Furthermore, due to the un-splitting treatment of photon transport and collision in the flux evaluation, the current IUGKS has asymptotic preserving property in the capturing of diffusion solution without imposing the constraint of mesh size being smaller than the photon mean free path. At the same time, accurate solutions can be obtained in the optically thin regime as well. For a single simulation with multiple regimes, the IUGKS can present a smooth transition from the optically thin to optically thick region with a variation of the ratio between the time step and local photon's collision time. The current scheme can recover the nine-point scheme in the diffusive limit on distorted quadrilateral mesh [17], and further reduce to the standard five-point scheme on orthogonal quadrilateral mesh. The numerical examples validate the current approach.

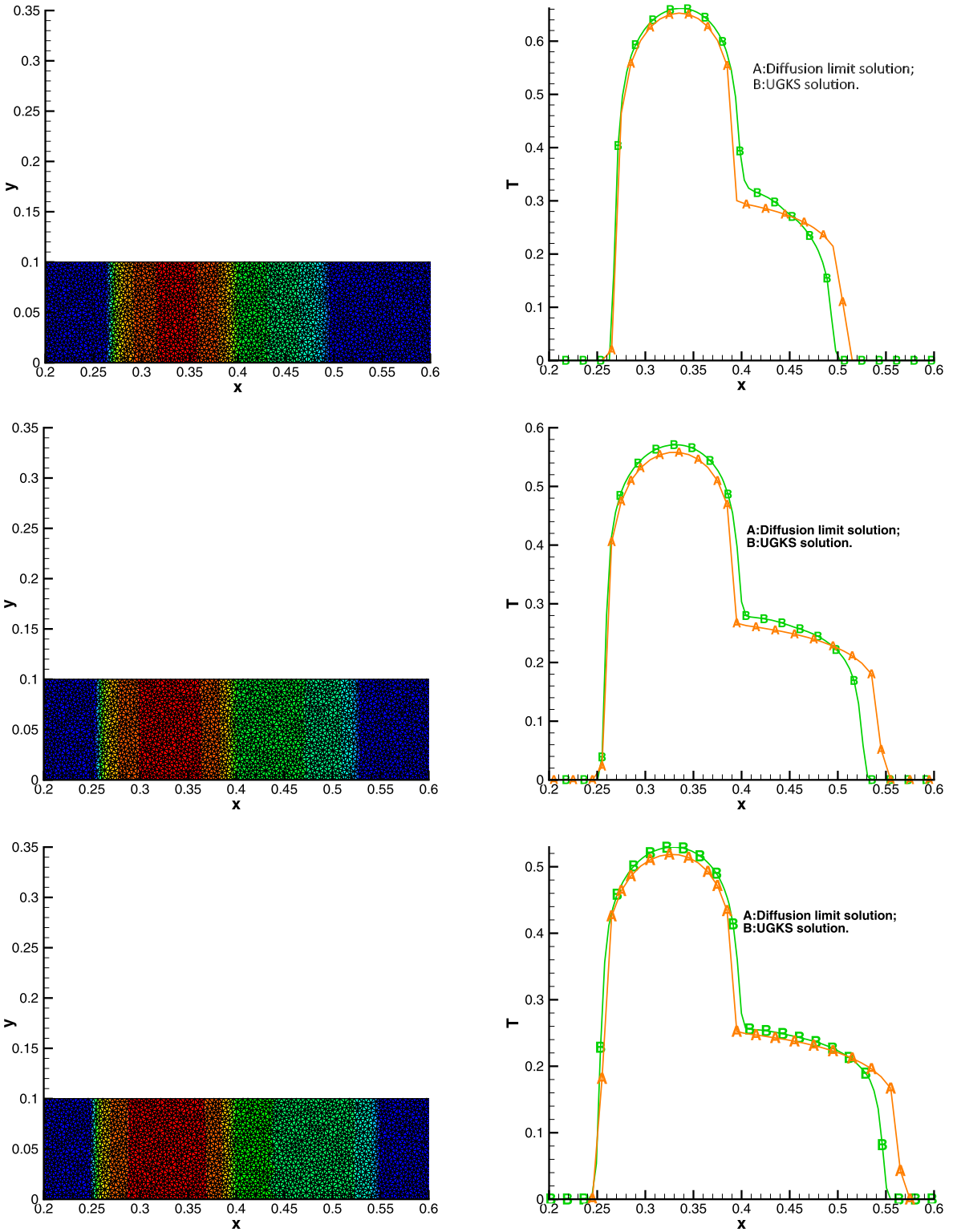

Fig. 6. The left is the contour of material temperature for problem three, and the right is the material temperature comparison with the result of the diffusion limit solution. From top to bottom, the result are at five simulation times of 4 ns, 12 ns and 20 ns respectively.

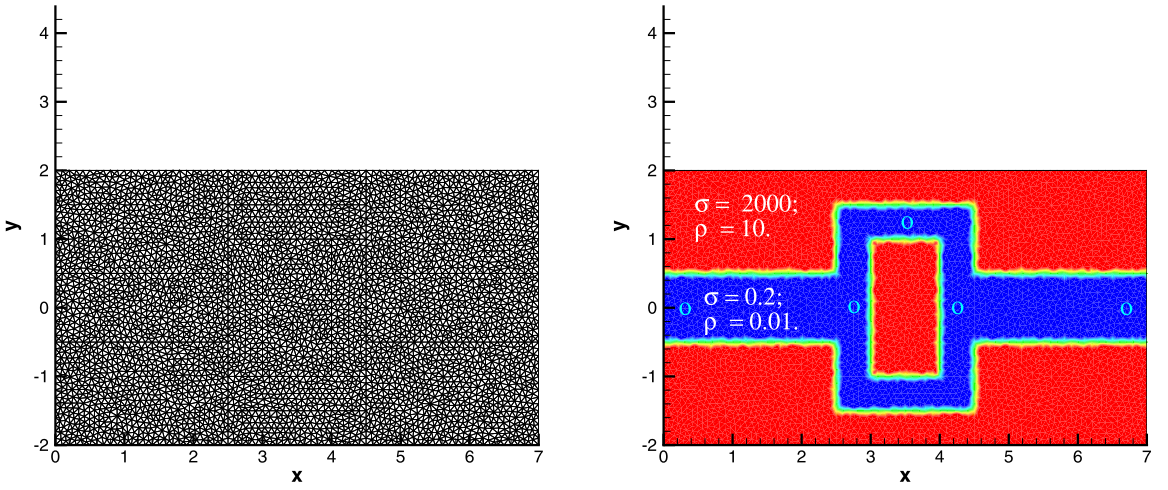

Fig. 7. The left is the unstructured mesh for Tophat test problem, and the right gives the initial opacity data and the locations of five probe points.

Acknowledgements

The authors wish to thank the referees for the useful suggestions which improve this paper. The work of Sun is supported by NSFC (Grant Nos. 11671048, 91630310, 11371068) and CAEP Project (2015B0202041, 2015B0202040). The research of Jiang is supported by the National Basic Research Program under Grant 2014CB745002 and NSFC (Grant Nos. 11229101, 11631008, 11371065). The work of Xu is supported by Hong Kong research grant council (16207715, 16211014, 620813) and NSFC-91330203 and 91530319.

Appendix A

In this appendix, we give the details of the derivation of formulae (3.14) to (3.16) in the step-by-step manner. First by using the reconstruction expressions (3.10) and (3.11), we get from (3.8) that

$$\begin{aligned} I_m(t,0,0,\mu_m',\xi_m') &= e^{-\vartheta_{j,k}(t-t^n)}\{(I_{j,k,m}^{-,'}1_{\mu_m'>0} + I_{j,k,m}^{+,'}1_{\mu_m'<0}) \\ &\quad - \tfrac{c}{\epsilon}(t-t^n)([\mu_m'(\delta_{x'}I)_{j,m}^{n+1} + \xi_m'(\delta_{y'}I)_{j,m}^{n+1}]1_{\mu_m'>0} + [\mu_m'(\delta_{x'}I)_{j_1,m}^{n+1} + \xi_m'(\delta_{y'}I)_{j_1,m}^{n+1}]1_{\mu_m'<0})\} \\ &\quad + \int_{t^n}^{t} e^{-\vartheta_{j,k}(t-s)}\tfrac{c\sigma_{j,k}}{2\pi\epsilon^2}\{\phi_{j,k}^{n+1} - \tfrac{c}{\epsilon}(t-s)[\mu_m'((\delta_{x'}\phi)_{j,k}^{n+1,-}1_{\mu_m'>0} + \\ &\quad (\delta_{x'}\phi)_{j,k}^{n+1,+}1_{\mu_m'<0}) + \xi_m'(\delta_{y'}\phi)_{j,k}^{n+1}] + (\delta_t\phi)_{j,k}^{n+1}(s-t^{n+1})\}ds, \end{aligned} \tag{A.1}$$

where $I_{j,k,m}^{-,'}, I_{j,k,m}^{+,'}$ are the boundary values

$$\begin{aligned} I_{j,k,m}^{-,'} &= I_{j,m}^{n+1} + (\delta_{x'}I)_{j,m}^{n+1}(-x_j^{c,'}) + (\delta_{y'}I)_{j,m}^{n+1}(-y_j^{c,'}), \\ I_{j,k,m}^{+,'} &= I_{j_1,m}^{n+1} + (\delta_{x'}I)_{j_1,m}^{n+1}(-x_{j_1}^{c,'}) + (\delta_{y'}I)_{j_1,m}^{n+1}(-y_{j_1}^{c,'}). \end{aligned}$$

Based on the above modeling, the numerical flux

$$F_{j,k,m} = \frac{cl_k}{\epsilon\Delta t}\int_{t^n}^{t^{n+1}} \mu_m' I_m(t,0,0,\mu_m',\xi_m')dt$$

can be exactly evaluated by using the expressions (A.1). So we can obtain

$$\begin{aligned} F_{j,k,m} &= l_k\{A_{j,k}\mu_m'(I_{j,k,m}^{-,'}1_{\mu_m'>0} + I_{j,k,m}^{+,'}1_{\mu_m'<0}) \\ &\quad + C_{j,k}\mu_m'\phi_{j,k}^{n+1} \\ &\quad + D_{j,k}[(\mu_m')^2((\delta_{x'}\phi)_{j,k}^{n+1,-}1_{\mu_m'>0} + (\delta_{x'}\phi)_{j,k}^{n+1,+}1_{\mu_m'<0}) + \mu_m'\xi_m'(\delta_{y'}\phi)_{j,k}^{n+1}] \\ &\quad + B_{j,k}([(\mu_m')^2(\delta_{x'}I)_{j,m}^{n+1} + \mu_m'\xi_m'(\delta_{y'}I)_{j,m}^{n+1}]1_{\mu_m'>0} + [(\mu_m')^2(\delta_{x'}I)_{j_1,m}^{n+1} + \mu_m'\xi_m'(\delta_{y'}I)_{j_1,m}^{n+1}]1_{\mu_m'<0}) \\ &\quad + E_{j,k}\mu_m'(\delta_t\phi)_{j,k}^{n+1}\}, \end{aligned} \tag{A.2}$$

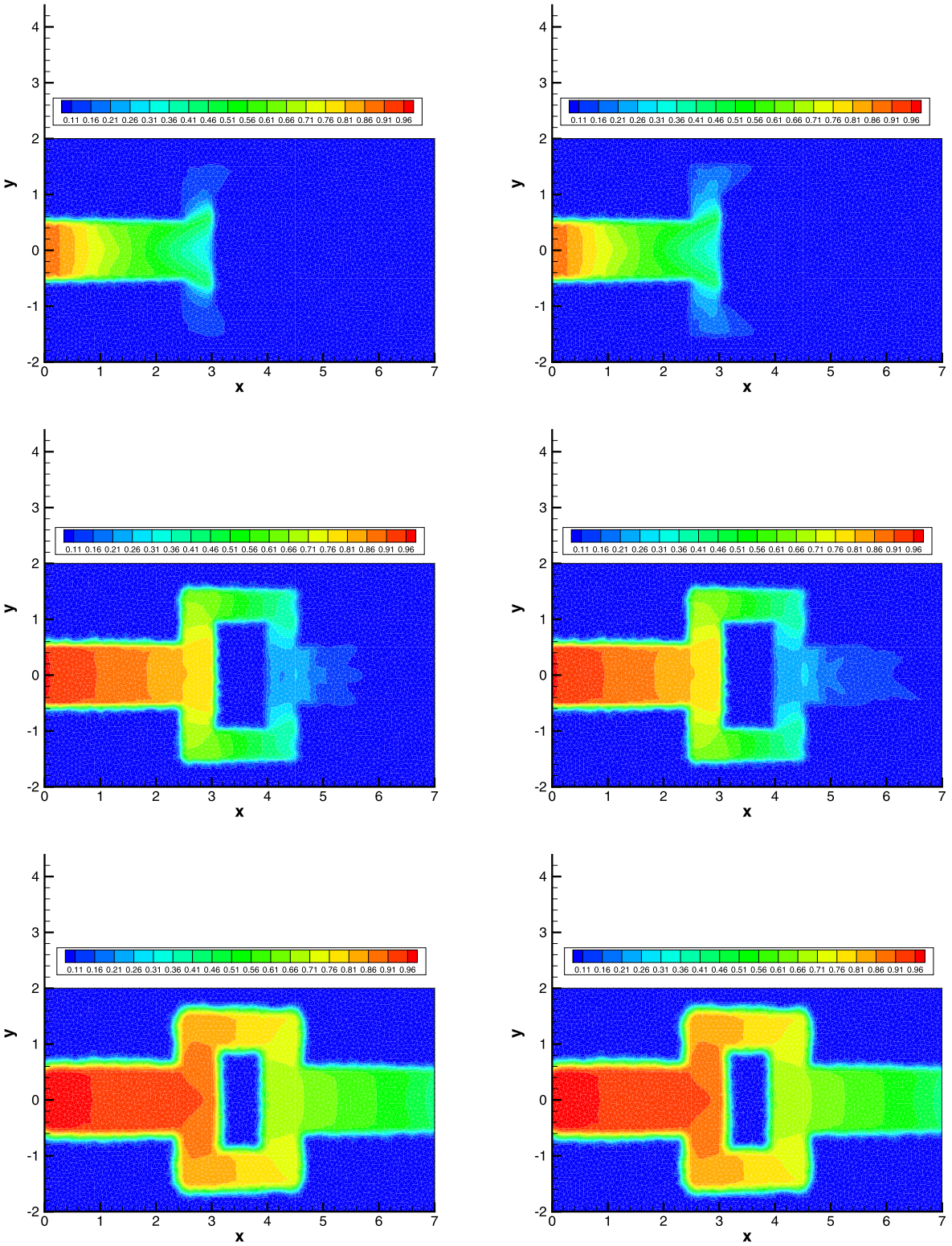

Fig. 8. The contour lines of material and radiation temperature of Tophat test problem at times 8 ns, 94 ns and 1000 ns from top to bottom respectively. The temperature unit is 0.5 keV. The left is the material temperature and right is the radiation temperature.

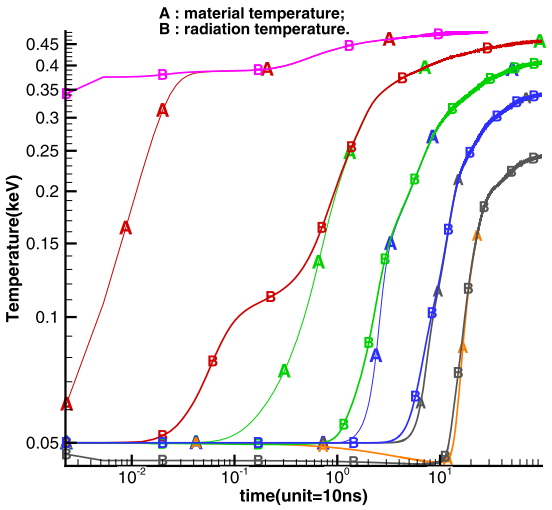

Fig. 9. The time evolution of material and radiation temperature at five probe points. In this figure, the unit of temperature is keV, and the unit for time is 10 ns. B: the radiation temperature; A: the material temperature.

and the coefficients in (A.2) are given by

$$
\begin{aligned}
A(\Delta t,\epsilon,\sigma,\vartheta) &= \tfrac{c}{\epsilon\Delta t}\int_{t^n}^{t^{n+1}} e^{-\vartheta(t-t^n)}dt = \tfrac{c}{\epsilon\Delta t\vartheta}(1-e^{-\vartheta\Delta t}),\\
C(\Delta t,\epsilon,\sigma,\vartheta) &= \tfrac{c}{\epsilon\Delta t}\int_{t^n}^{t^{n+1}}\int_{t^n}^{t} e^{-\vartheta(t-s)}\tfrac{c\sigma}{2\pi\epsilon^2}dsdt = \tfrac{c^2\sigma}{2\pi\Delta t\epsilon^3\vartheta}(\Delta t-\tfrac{1}{\vartheta}(1-e^{-\vartheta\Delta t})),\\
D(\Delta t,\epsilon,\sigma,\vartheta) &= \tfrac{c}{\epsilon\Delta t}\int_{t^n}^{t^{n+1}}\int_{t^n}^{t} e^{-\vartheta(t-s)}\tfrac{c\sigma}{2\pi\epsilon^2}(-\tfrac{c}{\epsilon}(t-s))dsdt\\
&= -\tfrac{c^3\sigma}{2\pi\Delta t\epsilon^4\vartheta^2}(\Delta t(1+e^{-\vartheta\Delta t})-\tfrac{2}{\vartheta}(1-e^{-\vartheta\Delta t})),\\
B(\Delta t,\epsilon,\sigma,\vartheta) &= \tfrac{c}{\epsilon\Delta t}\int_{t^n}^{t^{n+1}} e^{-\vartheta(t-t^n)}(-\tfrac{c}{\epsilon}(t-t^n))dt = -\tfrac{c^2}{\epsilon^2\vartheta^2\Delta t}(1-e^{-\vartheta\Delta t}-\vartheta\Delta t e^{-\vartheta\Delta t}),\\
E(\Delta t,\epsilon,\sigma,\vartheta) &= \tfrac{c}{\epsilon\Delta t}\int_{t^n}^{t^{n+1}}\int_{t^n}^{t} e^{-\vartheta(t-s)}\tfrac{c\sigma}{2\pi\epsilon^2}(s-t^{n+1})dsdt\\
&= \tfrac{c^2\sigma}{2\pi\epsilon^3\vartheta^3\Delta t}(1-e^{-\vartheta\Delta t}-\vartheta\Delta t e^{-\vartheta\Delta t}-\tfrac{1}{2}(\vartheta\Delta t)^2),
\end{aligned}
\tag{A.3}
$$

with $\vartheta = \frac{c\sigma}{\epsilon^2}$.

Finally the expressions in (A.2) have the following functional dependence,

$$
\begin{aligned}
A_{j,k} &= A(\Delta t,\epsilon,\sigma_{j,k}^{n+1},\vartheta_{j,k}^{n+1}),\\
C_{j,k} &= C(\Delta t,\epsilon,\sigma_{j,k}^{n+1},\vartheta_{j,k}^{n+1}),\\
D_{j,k} &= D(\Delta t,\epsilon,\sigma_{j,k}^{n+1},\vartheta_{j,k}^{n+1}),\\
B_{j,k} &= B(\Delta t,\epsilon,\sigma_{j,k}^{n+1},\vartheta_{j,k}^{n+1}),\\
E_{j,k} &= E(\Delta t,\epsilon,\sigma_{j,k}^{n+1},\vartheta_{j,k}^{n+1}).
\end{aligned}
\tag{A.4}
$$

References

[1] W.J. Sun, S. Jiang, K. Xu, An asymptotic preserving unified gas kinetic scheme for gray radiative transfer equations, J. Comput. Phys. 285 (2015) 265–279.
[2] S.Z. Chen, K. Xu, C.B. Lee, Q.D. Cai, A unified gas kinetic scheme with moving mesh and velocity space adaptation, J. Comput. Phys. 231 (2012) 6643–6664.
[3] N.A. Gentile, Implicit Monte Carlo diffusion – an acceleration method for Monte Carlo time-dependent radiative transfer simulations, J. Comput. Phys. 172 (2001) 543–571.
[4] J.C. Huang, K. Xu, P.B. Yu, A unified gas-kinetic scheme for continuum and rarefied flows II: multi-dimensional cases, Commun. Comput. Phys. 12 (3) (2012) 662–690.
[5] S. Jin, C.D. Levermore, The discrete-ordinate method in diffusive regimes, Transp. Theory Stat. Phys. 20 (5–6) (1991) 413–439.
[6] S. Jin, C.D. Levermore, Fully discrete numerical transfer in diffusive regimes, Transp. Theory Stat. Phys. 22 (6) (1993) 739–791.
[7] S. Jin, L. Pareschi, G. Toscani, Uniformly accurate diffusive relaxation schemes for multiscale transport equations, SIAM J. Numer. Anal. 38 (3) (2000) 913–936.
[8] A. Klar, An asymptotic-induced scheme for nonstationary transport equations in the diffusive limit, SIAM J. Numer. Anal. 35 (6) (1998) 1073–1094.
[9] A.W. Larsen, J.E. Morel, Asymptotic solutions of numerical transport problems in optically thick, diffusive regimes. II, J. Comput. Phys. 83 (1) (1989) 212–236.

[10] A.W. Larsen, J.E. Morel, W.F. Miller Jr., Asymptotic solutions of numerical transport problems in optically thick, diffusive regimes, J. Comput. Phys. 69 (2) (1987) 283–324.
[11] E.W. Larsen, G.C. Pomraning, V.C. Badham, Asymptotic analysis of radiative transfer problems, J. Quant. Spectrosc. Radiat. Transf. 29 (1983) 285.
[12] C.E. Lee, The Discrete S_N Approximation to Transport Theory, LA-2595, 1962.
[13] L. Mieussens, On the asymptotic preserving property of the unified gas kinetic scheme for the diffusion limit of linear kinetic model, J. Comput. Phys. 253 (2013) 138–156.
[14] V. Venkatakrishnan, Convergence to steady state solutions of the Euler equations on unstructured grids with limiters, J. Comput. Phys. 118 (1995) 120–130.
[15] K. Xu, J.C. Huang, A unified gas-kinetic scheme for continuum and rarefied flows, J. Comput. Phys. 229 (2010) 7747–7764.
[16] W.J. Sun, S. Jiang, K. Xu, S. Li, An asymptotic preserving unified gas kinetic scheme for frequency-dependent radiative transfer equations, J. Comput. Phys. 302 (2015) 222–238.
[17] Z.Q. Sheng, G.W. Yuan, A nine point scheme for the approximation of diffusion operators on distorted quadrilateral meshes, SIAM J. Sci. Comput. 30 (2008) 1341–1361.
[18] W.J. Sun, Q.H. Zeng, S.G. Li, The asymptotic preserving unified gas kinetic scheme for gray radiative transfer equations on distorted quadrilateral meshes, Ann. Differ. Equ. (02) (2016) 141–165.
[19] D. Balsara, Fast and accurate discrete ordinates methods for multidimensional radiative transfer. Part I, basic methods, J. Quant. Spectrosc. Radiat. Transf. 69 (2001) 671–707.
[20] W.J. Sun, S. Jiang, K. Xu, An implicit unified gas kinetic scheme for radiative transfer with equilibrium and non-equilibrium diffusive limits, Commun. Comput. Phys. 22 (2017) 889–912.